

See discussions, stats, and author profiles for this publication at: <https://www.researchgate.net/publication/266254911>

Structural Basis for Inhibition of Mycobacterial and Human Adenosine Kinase by 7-Substituted 7-(Het)aryl-7-deazaadenine Ribonucleosides

ARTICLE in JOURNAL OF MEDICINAL CHEMISTRY · SEPTEMBER 2014

Impact Factor: 5.45 · DOI: 10.1021/jm500497v · Source: PubMed

CITATIONS

3

READS

71

20 AUTHORS, INCLUDING:



Jiří Brynda

Institute of Molecular Genetics AS CR

91 PUBLICATIONS 1,086 CITATIONS

[SEE PROFILE](#)



Aurelie Bourderioux

14 PUBLICATIONS 117 CITATIONS

[SEE PROFILE](#)



Radek Pohl

Academy of Sciences of the Czech Republic

220 PUBLICATIONS 3,683 CITATIONS

[SEE PROFILE](#)



Václav Veverka

Academy of Sciences of the Czech Republic

48 PUBLICATIONS 656 CITATIONS

[SEE PROFILE](#)

Structural Basis for Inhibition of Mycobacterial and Human Adenosine Kinase by 7-Substituted 7-(Het)aryl-7-deazaadenine Ribonucleosides

Jan Snášel,^{†,‡} Petr Nauš,^{†,‡} Jiří Dostál,[†] Aleš Hnizda,[†] Jindřich Fanfrlík,[†] Jiří Brynda,[†] Aurelie Bourderioux,[†] Michal Dušek,[‡] Hana Dvořáková,[§] Jiřina Stolaříková,^{||} Helena Zábranská,[†] Radek Pohl,[†] Petr Konečný,[⊥] Petr Džubák,[⊥] Ivan Votruba,^{†,∞} Marián Hajdúch,[⊥] Pavlína Řezáčová,[†] Václav Veverka,[†] Michal Hocek,^{*,†} and Iva Pichová^{*,†}

[†]Institute of Organic Chemistry and Biochemistry, Academy of Sciences of the Czech Republic, Flemingovo nam. 2, 16610 Prague 6, Czech Republic

[‡]Institute of Physics ASCR, v.v.i., Na Slovance 2, 182 21 Praha 8, Czech Republic

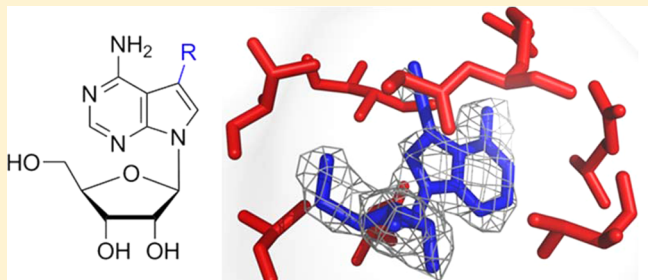
[§]Laboratory of NMR Spectroscopy, Institute of Chemical Technology, Technická 5, 16628 Prague 6, Czech Republic

^{||}Laboratory for Mycobacterial Diagnostics and Tuberculosis, Regional Institute of Public Health in Ostrava, Partyzánské nám. 7, 70200 Ostrava, Czech Republic

[⊥]Institute of Molecular and Translational Medicine, Faculty of Medicine and Dentistry, Palacky University and University Hospital in Olomouc, Hněvotínská 5, 77515 Olomouc, Czech Republic

S Supporting Information

ABSTRACT: Adenosine kinase (ADK) from *Mycobacterium tuberculosis* (Mtb) was selected as a target for design of antimycobacterial nucleosides. Screening of 7-(het)aryl-7-deazaadenine ribonucleosides with Mtb and human (*h*) ADKs and testing with wild-type and drug-resistant Mtb strains identified specific inhibitors of Mtb ADK with micromolar antimycobacterial activity and low cytotoxicity. X-ray structures of complexes of Mtb and *h*ADKs with 7-ethynyl-7-deazaadenosine showed differences in inhibitor interactions in the adenosine binding sites. 1D ¹H STD NMR experiments revealed that these inhibitors are readily accommodated into the ATP and adenosine binding sites of Mtb ADK, whereas they bind preferentially into the adenosine site of *h*ADK. Occupation of the Mtb ADK ATP site with inhibitors and formation of catalytically less competent semiopen conformation of MtbADK after inhibitor binding in the adenosine site explain the lack of phosphorylation of 7-substituted-7-deazaadenosines. Semiempirical quantum mechanical analysis confirmed different affinity of nucleosides for the Mtb ADK adenosine and ATP sites.



R = ethynyl inhibitors of *h*ADK and Mtb ADK; cytotoxic
R = small hetaryl selective inhibitor of Mtb ADK, non-cytotoxic

INTRODUCTION

Tuberculosis (TB) remains one of the leading public health problems worldwide and is more prevalent in the world today than at any other time in human history. In 2012, an estimated 8.6 million people developed TB, and 1.3 million died from the disease (WHO tuberculosis report 2013). In recent decades, multidrug-resistant (MDR) and even more ominous extensively drug-resistant (XDR) *Mycobacterium tuberculosis* (Mtb) strains have emerged.¹ At the same time, a high rate of HIV co-infection, especially in developing countries, has increased the susceptibility of the population to Mtb infection. Successful treatment of TB requires long courses of several antibiotics. In HIV-positive patients, TB treatment is further complicated by undesirable drug–drug interactions that decrease the therapeutic concentration of antiretrovirals by induction of the

hepatic cytochrome P450 oxidase system.² Similar restrictions apply to coadministration of diabetes and TB drugs. Mtb can persist permanently in host lesions, evading immune surveillance. An estimated one-third of the world's population asymptotically harbors a latent form of Mtb, with a life-long risk of disease activation and transmission. However, existing drugs do not target the latent form of Mtb. Therefore, the discovery of new molecules with new mechanisms of action is needed to address latent Mtb. New treatments may become critical as MDR and XDR Mtb incidence increases.

Enzymes involved in the biosynthesis of purine nucleotides are potential targets for development of new types of

Received: March 28, 2014

Published: September 26, 2014



compounds active against Mtb. In most organisms, purine nucleotides are formed from purine bases and phosphoribosyl 1-pyrophosphate or by phosphorylation of nucleosides in the purine salvage pathway, or they are synthesized de novo in a multistep sequence. Mtb expresses enzymes from both pathways; however, the interdependence and regulation of these processes remain unclear. Of the variety of possible target enzymes from the Mtb purine salvage pathway,^{3,4} adenosine kinase (ADK, EC 2.7.1.20, Rv2202c)⁵ is considered a promising target for drug development. ADK catalyzes phosphorylation of adenosine to adenosine monophosphate (AMP) in the phosphoryl transfer reaction using adenosine 5'-triphosphate (ATP) as a substrate and releasing adenosine 5'-diphosphate (ADP). ADK is present in most eukaryotes, fungi, plants, and parasites but is not commonly found in bacteria. The activity of ADK has been confirmed in Mtb,⁶ and biochemical characterization indicates that this enzyme shares low structural similarity with and behaves very differently from human and other well-characterized ADKs.^{3,7}

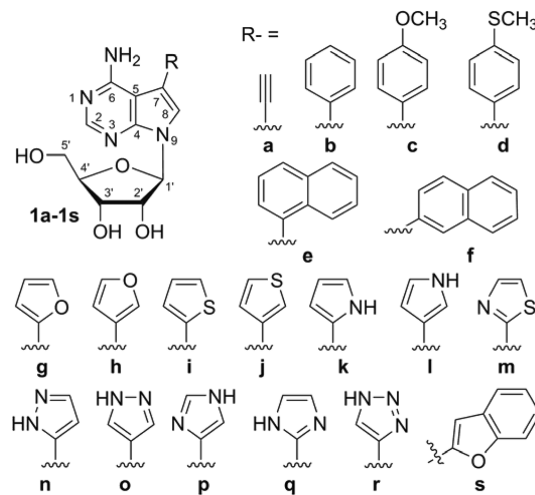
Nucleoside analogs are an important group of drugs used to treat viral infections and cancer. Certain nucleoside inhibitors are active against *Toxoplasma gondii*⁸ and other parasites.⁹ Several adenosine analogs with various modifications have already been tested for inhibition of Mtb ADK.^{3,6,10} These studies established the promise of these compounds for drug development. In addition, diverse modified 7-deazapurine nucleosides have been reported as ADK inhibitors.^{11–15} Recently, we discovered 6-hetaryl-7-deazapurine ribonucleosides with nanomolar cytostatic activities toward leukemia and cancer cell lines,¹⁶ and we later found that these nucleosides are excellent inhibitors of Mtb ADK but only weak antimycobacterial agents.¹⁷ Related 7-deazaadenosines bearing small five-membered heterocycles at position 7 (**1**) were also found to be nanomolar cytostatics,¹⁸ whereas compounds bearing bulky aromatic substituents were neither cytostatic nor cytotoxic. Here, we report on the structure–activity relationship of 7-substituted 7-(het)aryl-7-deazaadenine ribonucleosides with Mtb ADK and human ADK (*h*ADK). We also describe screening of these compounds for in vitro inhibition of Mtb ADK and *h*ADK and for inhibition of two Mtb strains.

■ RESULTS AND DISCUSSION

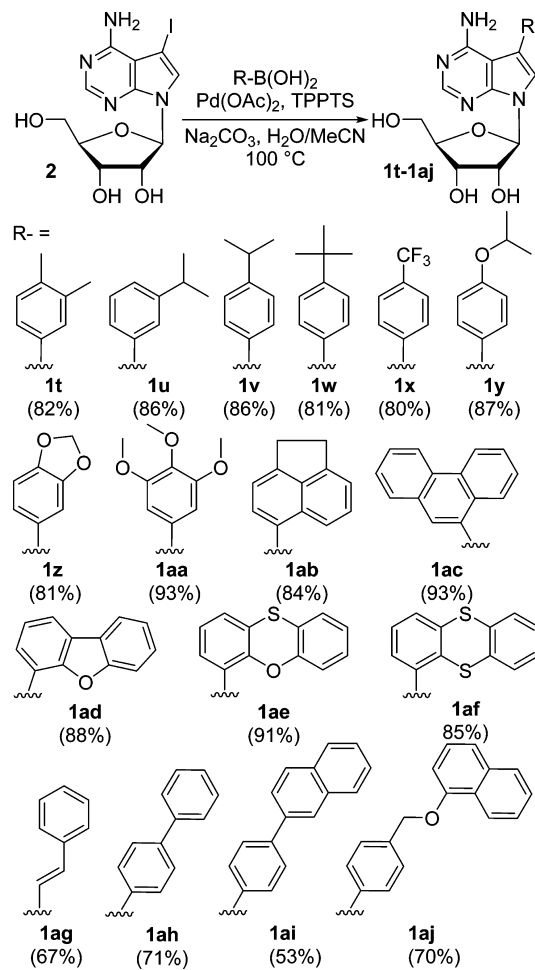
Chemistry of 7-Substituted 7-Deazaadenosines. Synthesis of **1a–s** (Chart 1) was reported previously.¹⁸ Our previous study showed that 7-deazaadenosine derivatives bearing small five-membered rings or acetylene exerted significant cytostatic/cytotoxic effects. To identify nontoxic derivatives with potential activity against Mtb ADK, we designed a series of nucleosides bearing bulky hydrophobic aromatic substituents at position 7. These substituents included substituted benzenes (**1t–aa**), polycyclic (hetero)aromatics (**1ab–af**), styrene (**1ag**), biaryls (**1ah,ai**), and aryl benzyl ether (**1aj**). All compounds were prepared by a single-step procedure based on the aqueous Suzuki–Miyaura cross-coupling reactions of 7-iodo-7-deazaadenosine (**2**) with the corresponding arylboronic acids (Scheme 1). The reactions generally proceeded smoothly, providing the desired 7-aryl-7-deazaadenosines **1t–aj** in good yields of 67–91% (with the exception of compound **1ai**, which was isolated in 53% yield).

Biological Activity Profiling of 7-Substituted 7-Deazapurine Derivatives. Compounds **1a–aj** were tested for inhibition of human and Mtb ADKs (for cloning, expression, and purification of these enzymes, see ref 19).

Chart 1. Numbering of Proton Positions in Modified Nucleosides and Structures of Previously Reported 7-Substituted 7-Deazaadenosines



Scheme 1. Synthesis of 7-Deazaadenosines Bearing Bulky Substituents at Position 7



Most compounds were also tested as potential kinase substrates. The inhibition and substrate phosphorylation screening results were correlated with the compounds' in vitro cytotoxicity (MTT) against nonmalignant BJ and MRC-5 human fibroblast cell lines (Table 1). As expected, the

Table 1. Cytotoxicity, Human and Mtb ADK Inhibition, and Antimycobacterial Activity

compd	BJ ^a CC ₅₀ (μM)	MRC-5 CC ₅₀ (μM)	ADK Phs ^b (%), human	ADK inhibition IC ₅₀ (μM)		M. bovis ^c IC ₅₀ (μM)	M. tuberculosis ^d MIC (μM)	
				human	Mtb		My 331/88	Praha 131
1a	43.1 ± 3.6	13.4 ± 3.6	62	0.20 ± 0.02	0.33 ± 0.02	0.13	8	8
1b	50.9 ± 6.4	21.0 ± 3.2		>5	>10	1.34	8	8
1c	21.9 ± 1.4	61.4 ± 6.1		>5	>10	2.08	16	16
1d	18.0 ± 3.2	45.6 ± 3.5		>10	>10	0.36	4	8
1e	90.6 ± 5.8	94.4 ± 8.7		>10	>10	1.87	32	32
1f	13.9 ± 1.9	13.6 ± 1.5		>5	5.33 ± 0.65	0.39	2	4
1g	18.3 ± 2.1	9.49 ± 1.49	8	>5	2.10 ± 0.15	17.4	62.5	62.5
1h	91.5 ± 13.3	67.9 ± 14.9	9	>5	>10	8.31	16	16
1i	65.4 ± 2.6	39.4 ± 4.5	2	>5	>10	4.73	8	8
1j	12.9 ± 0.9	42.5 ± 5.3	2	>5	6.60 ± 0.51	3.93	8	8
1k	>100	99.6 ± 1.0	6	>20	4.4 ± 0.30	7.27	62.5	62.5
1l	10.1 ± 1.5	5.05 ± 0.88	20	4.5 ± 0.31	>10	1.12	62.5	62.5
1m	>100	25.1 ± 5.1	3	2.3 ± 0.17	4.5 ± 0.20	2.51	125	125
1n	9.51 ± 2.03	0.18 ± 0.13	7	>10	>10	48.0	>250	>250
1o	48.9 ± 5.3	71.2 ± 8.9	9	>10	>5	3.08	125	125
1p	0.12 ± 0.03	0.33 ± 0.04	47	13	>10	>100	>250	>250
1q	1.48 ± 0.28	0.15 ± 0.06	19	>20	>3	>100	>250	>250
1r	0.08 ± 0.02	0.10 ± 0.0	37	>20	>10	69.0	>250	>250
1s	21.2 ± 2.1	35.1 ± 3.8		>10	1.80 ± 0.20	2.27	16	16
1t	57.3 ± 1.4	37.9 ± 2.8		>20	4.9 ± 0.40	1.13	8	8
1u	>100	>100		3.3 ± 0.4	2.33 ± 0.25	6.75	32	32
1v	63.9 ± 4.4	52.9 ± 8.7		>20	>10	5.29	16	16
1w	>100	96.3 ± 5.9		>20	>10	4.54	62.5	62.5
1x	62.0 ± 9.1	78.8 ± 12.0		>10	>10	1.16	4	4
1y	59.9 ± 2.7	50.2 ± 8.8		>10	13.1 ± 1.5	3.07	32	32
1z	15.5 ± 0.7	46.0 ± 8.1		>10	>10	1.38	8	8
1aa	>100	>100		>10	>10	7.05	8	8
1ab	23.1 ± 2.5	>100		>10	>10	1.74	16	16
1ac	>100	66.0 ± 9.2		>10	>10	1.90	32	32
1ad	>100	100 ± 0.08		>10	0.6 ± 0.05	0.19	4	4
1ae	>100	95.1 ± 7.7		>20	0.3 ± 0.02	4.53	16	16
1af	>100	68.5 ± 6.3		>10	2.06 ± 0.14	44.32	62.5	125
1ag	19.6 ± 1.7	48.2 ± 9.6		>10	0.9 ± 0.12	1.30	8	8
1ah	40.6 ± 7.9	93.7 ± 6.5		>20	7.67 ± 0.81	1.68	4	4
1ai	0.12 ± 0.03	64.2 ± 12.1		>20	>10	74.42	62.5	62.5
1aj	>100	92.1 ± 12.5		>20	>10	6.39	16	32

^aCytotoxicity (MTT test) in BJ and MRC-5 fibroblasts. ^bPhs, ADK substrate activity (phosphorylation), conversion to 5'-phosphate (%). ^c50% growth inhibitory concentration of *Mycobacterium bovis* BCG cultivated in vitro. ^dIncubation time = 14 days. MIC of isoniazid as reference compound was 0.5 μM for the My 331/88 strain.

cytotoxicity strongly depended on the bulkiness of the substituent at position 7, with all compounds bearing bulky groups showing little to no cytotoxicity (with the exception of **1ai**, which was toxic to BJ cells). Most compounds did not significantly inhibit hADK and were poor-to-moderate substrates for this enzyme. Only the 7-ethynyl derivative (**1a**) was a potent (submicromolar) hADK inhibitor, while a few additional derivatives (**1l,m,u**) were inhibitory at micromolar concentrations. In contrast, most derivatives (e.g., **1f,g,j,k,m,s,t,u,y,af,ah**) showed significant inhibition of Mtb ADK with IC₅₀ values in the micromolar range. Three bulky derivatives (**1ad,ae,ag**) inhibited the Mtb enzyme at sub-micromolar concentrations but showed no inhibitory activity toward hADK. All compounds were also tested for activity against *Mycobacterium bovis* and Mtb (strain My 331/88 and drug-resistant strain Praha 131). Most compounds, except **1n–r**, were active against Mtb with in vitro minimum inhibitory concentration (MIC) ranging between 2 and 60 μM (see Table

1). The antimycobacterial activities of 14 compounds from our series of 39 nucleoside analogs correlated well with Mtb ADK inhibition. We found that **1d,i,x,aa,ab,ac,aj** were fairly active against Mtb and *M. bovis* but did not inhibit Mtb and hADKs, perhaps suggesting that they can target other enzymes from the purine salvage pathway. The Mtb-ADK-specific derivative **1f** (7-(2-naphthyl)) displayed the highest antimycobacterial activity with MIC of 2 and 4 μM for the wild-type and drug-resistant Mtb strains, respectively. The nontoxic, Mtb-ADK-specific dibenzofuran derivative (**1ad**) showed the best therapeutic index. This compound displayed antimycobacterial activity with MIC of 4 μM for both Mtb strains. Compounds **1f** and **1ad** are promising lead structures for further development of antimycobacterial drugs. The lower activities of 7-deazapurine derivatives against Mtb compared to *M. bovis* could be the result of slightly different conditions used for cultivation and testing and/or the extent of compound uptake through the cell

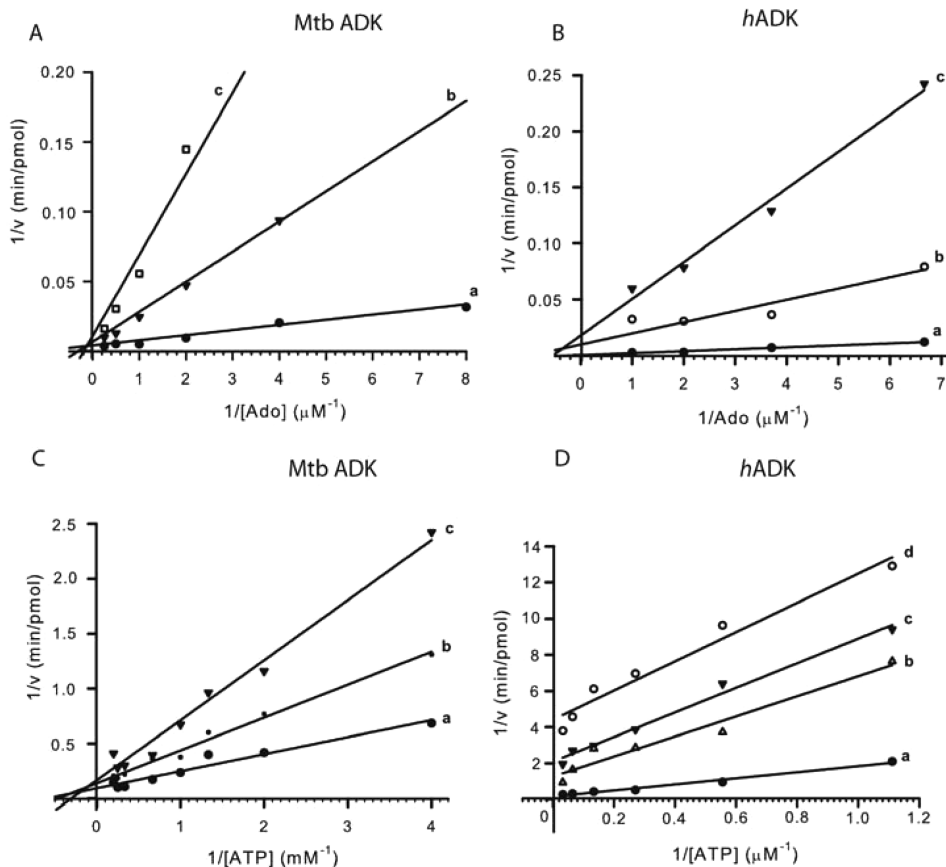


Figure 1. Kinetics of competition of **1a** with adenosine and ATP in Mtb ADK and *h*ADK binding sites. The panels show the Lineweaver–Burk plots: (A) inhibition of Mtb ADK in the presence of increasing concentrations of adenosine (Ado) (a, 0 μ M; b, 0.5 μ M; c, 1 μ M) and 5 mM ATP; (B) inhibition of *h*ADK in the presence of increasing concentrations of Ado (a, 0 nM; b, 20 nM; c, 30 nM) and 120 μ M ATP; (C) inhibition of Mtb ADK in the presence of increasing concentrations of ATP (a, 0 mM; b, 0.25 mM; c, 0.5 mM) and 5 μ M Ado; (D) inhibition of *h*ADK in the presence of increasing concentrations of ATP (a, 0 nM; b, 15 nM; c, 30 nM; d, 60 nM) and 5 μ M Ado.

wall. Therefore, our future focus will be on design of suitable prodrugs and delivery of nucleosides.

We observed differences in phosphorylation of 7-substituted 7-deazapurine nucleosides by human and Mtb ADK. While no synthesized analog was phosphorylated by Mtb ADK, several compounds served as substrates for *h*ADK (see Table 1). This may indicate differences in the structures of these enzymes and/or different binding modes of nucleoside analogs into the adenosine and ATP binding sites.

To gain insight into the mechanism of action of 7-substituted 7-deazapurine nucleosides on *h*ADK and Mtb ADK, the kinetics of compound **1a**, which inhibits both ADKs but is phosphorylated only by *h*ADK, were examined. For both enzymes, the Lineweaver–Burk double reciprocal plots of initial velocities against increasing concentrations of adenosine indicated mixed competitive inhibition (Figure 1A,B) with **1a**, suggesting inhibitor binding into either the adenosine or ATP binding sites (or simultaneously to both sites) with almost comparable affinities. The plots from competition of **1a** with ATP in Mtb ADK also showed mixed competitive inhibition (Figure 1C), but for *h*ADK nearly parallel lines for increasing concentration of ATP were detected (Figure 1D). This type of inhibition can be interpreted as a mixed uncompetitive inhibition, which suggests preferential binding of inhibitor into the already formed complex between the enzyme and ATP; however, it does not exclude binding of **1a** into the ATP site.

Crystal Structures of *h*ADK-**1a** and Mtb ADK-**1a** Complexes.

To explore the binding of 7-substituted 7-deazapurine nucleosides to human and mycobacterial ADKs on a structural level, we determined crystal structures of *h*ADK and Mtb ADK in complex with **1a**, a compound that efficiently inhibits both enzymes and is specifically phosphorylated by *h*ADK.

The *h*ADK-**1a** complex crystallized in the $P2_12_12$ space group with two protein molecules in the asymmetric unit. The crystallographic model was refined to 2.5 Å resolution. Three molecules of **1a** were modeled into a well-defined electron density map (Figure S1 in Supporting Information). In both *h*ADK molecules in the asymmetric unit, **1a** binds into the substrate binding site located at the interface between a large core domain and a small lid domain. The position of **1a** mimics that of adenosine found in the crystal structure of the *h*ADK–adenosine complex (PDB code 1BX4).²⁰ The overall structure of the *h*ADK-**1a** complex is very similar to that of the adenosine bound enzyme. The protein adopts a closed conformation in which the small lid domain closes over the active site. Compound **1a** is completely buried in a hydrophobic pocket formed by amino acid residues Leu16, Leu40, Leu134, Ala 136, Leu138, and Phe170 (Figure 2A). The position of the base ring moiety is stabilized by a stacking interaction with the Phe170 side chain. The ethynyl moiety of **1a** is buried deep in the hydrophobic pocket and takes the place of a water molecule observed in the structure of *h*ADK with bound adenosine.

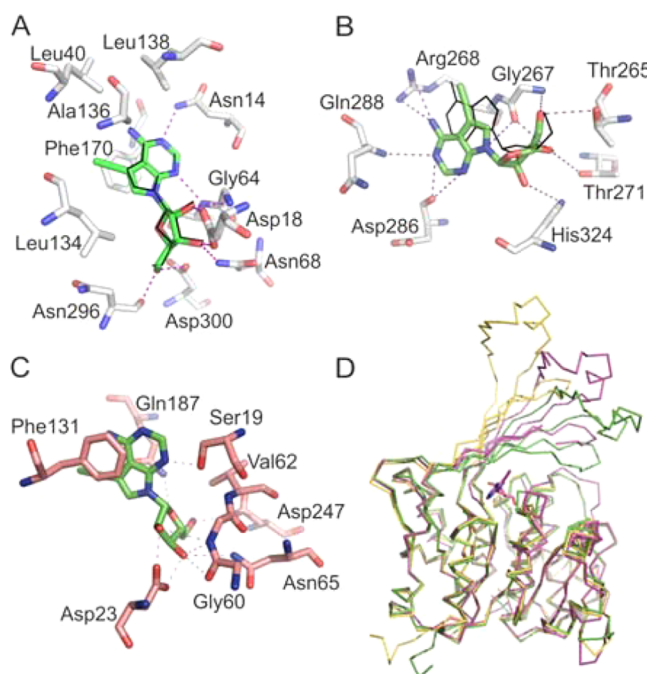


Figure 2. Binding of **1a** to the adenosine binding site (A) and ATP binding site (B) of *hADK* and to Mtb ADK (C). Residues interacting with **1a** are shown as sticks. Polar interactions are shown by magenta dashed lines. Adenosine positions superposed from crystal structures of *hADK*–adenosine (PDB code 1BX4)²⁰ or Mtb ADK–adenosine (PDB code 2PKM)²¹ complexes are represented as black lines. Panel D shows superposition of the semiopen conformation of the Mtb ADK–**1a** complex (magenta) with the open conformation of Mtb ADK apo form (yellow, PDB code 2PKF) and the closed conformation of the Mtb ADK–adenosine complex (green, PDB code 2PKM).

Similar replacement of a water molecule by an iodine atom was also observed for 5-iodo-5'-deoxytubericidin (PDB code 2I6A).⁷ The ribose ring of **1a** forms numerous direct hydrogen bonds with residues Asn14, Asp18, Gly64, Asn68, Asn296, and Asp300 (Figure 2A).

In one of the *hADK* molecules in the asymmetric unit (protein chain A), an additional molecule of **1a** is bound in the ATP binding site located in the core domain about 15 Å from the adenosine binding site. Partial occupancy within the asymmetric unit points to a lower affinity of this site for **1a**. The following amino acid residues form polar contacts with **1a**: Thr265, Gly267, Arg268, Thr271, Asp286, Gln288, and His324 (Figure 1B). The pose of **1a** closely resembles the binding of adenosine molecule into ATP binding site as found in the

structure of the *hADK*–adenosine complex (PDB code 1BX4).²⁰ The positions of the sugar moieties of **1a** and adenosine are very similar, but the positions of the bases are different. Interestingly, a loop surrounding the ATP binding site (and connecting β 14 to α 11) is partially disordered in the *hADK*–**1a** structure, and amino acid residues 286–292 could not be modeled into a continuous electron density map.

The Mtb ADK–**1a** complex crystallized in the *P*3₁ space group with two protein molecules per asymmetric unit representing the biologically relevant Mtb ADK dimer. The final crystallographic model was refined to 2.5 Å resolution with two molecules per asymmetric unit. The quality of electron density map for residues 9–48 and 99–120 is limited suggesting that the lid domain region is partially disordered. One molecule of **1a** bound to the enzyme active site was modeled into a well-defined electron density map in both molecules in the asymmetric unit (Figure S1). A molecule of **1a** binds into the adenosine binding pocket located at the interface of the core and lid domains; the ATP binding site remains unoccupied. Compound **1a** is deeply buried in the enzyme's active site, and its position is similar to that of adenosine (Figure 2C). The base ring moiety forms a stacking interaction with Phe131, and N1 engages in a polar interaction with the side chain of Ser19. The ethynyl moiety of **1a** makes a small number of van der Waals interactions with the hydrophobic side chains of Phe115 and Phe131. The ribose ring of **1a** forms numerous direct hydrogen bonds with the side chains of Asp23, Asn65, Gln187, and Asp274 and the main chain of Gly60 (Figure 2C). The lid domain (residues 9–48 and 99–120) adopts a unique conformation in the Mtb ADK–**1a** complex. While the conformation of the lid domain is open in the free or ATP-bound enzyme, it adopts a closed conformation upon binding of adenosine in *hADK*²⁰ and 2-fluoroadenosine, the only inhibitor for which the MtbADK complex structure is available (PDB code 2PKK).²¹ The conformation of the lid domain in the Mtb ADK–**1a** complex structure can be described as semiopen, because its position is between the open and closed states (Figure 2D). When the closed conformation of the lid is superposed on the Mtb ADK–**1a** complex structure, steric clashes occur between the ethynyl moiety of **1a** and residues Ser130, Phe131, and Phe115. We can therefore conclude that binding of **1a** prevents formation of catalytically competent arrangement of the closed enzyme. This can serve as a structural explanation for the observation that **1a** is not phosphorylated by Mtb ADK.

Competition of 7-Substituted 7-Deazapurine Derivatives with Adenosine and ATP in Mtb and Human Adenosine Kinases. We used 1D ¹H STD NMR experiments

Table 2. Relative STD Enhancements of Substrate (Adenosine or ATPγS) and Inhibitor Signals in the Presence of *hADK* or Mtb ADK^a

relative STD enhancement (%)															
<i>hADK</i>							Mtb ADK								
	Ado	ATP	1a	1m	1u	1ae	1g		Ado	ATP	1a	1m	1u	1ae	1g
H-1'	100	100	100	100	100	100	100		100	100	100	100	100	100	100
H-2	8	<1	33	57	72	33	64		44	57	63	37	42	50	43
H-8	20	<1	17	41	72	39	36		58	24	54	33	42	68	29
Ar				52	52	60	74					34	37	83	38
Ar'				78			67					45			31
Ar"							78								39

^aConcentration of all nucleosides was kept at the 500 μM.

to establish the mode of competition of 7-hetaryl-7-deazapurine derivatives with adenosine and ATP γ S for their respective binding sites and also to define the binding epitopes of the newly developed inhibitors.

First, we examined the binding behavior and mutual competition of adenosine and ATP γ S to *hADK* and Mtb ADK. For adenosine in the presence of *hADK*, the strongest enhancement was observed for the signal from H-1' and weaker enhancements for two aromatic proton signals H-8 and H-2 of ~20% and ~8% relative to H-1' (Table 2), which suggests that protons H-1' and H-8 are in closer contact with the protein than the rest of the substrate molecule. An analogous experiment for ATP γ S yielded much weaker absolute STD enhancements, which were limited to H-1' and NH₂. In addition, the STD enhancements induced by binding to *hADK* of both substrates were not significantly affected in spectra obtained from their equimolar mixture, which indicates that adenosine and ATP γ S do not compete and bind into their original binding sites.

The STD spectra for adenosine in the presence of Mtb ADK yielded maximum enhancement for H-1' and moderate enhancement for H-8 and H-2 of ~58% and ~44% (Figure 3A, Table 2), suggesting a similar contact epitope to that observed for *hADK*. The overall STD enhancement for ATP γ S

in the presence of Mtb ADK was comparable to that of adenosine, again with H-1' being the most affected proton (Figure 3B, Table 2). However, certain differences were found for the remaining ATP γ S protons in comparison with their binding to *hADK*. There was a very weak enhancement of the NH₂ signal (<5%), and the H-2 STD signal (~57%) was stronger than the H-8 signal (~24%). Importantly, simultaneous addition of adenosine and ATP γ S to MtbADK led to a dramatic reduction in the ATP γ S enhancements, suggesting direct competition between binding of adenosine and ATP γ S, as illustrated in Figure 3C. Intracellular ATP levels are generally in the low millimolar range, and adenosine is present at micromolar concentrations.^{22–28} Therefore, we can speculate that ATP binds into Mtb ADK first, and conformational changes in ADK allow adenosine binding and phosphorylation in bacteria.

We then selected compounds containing either smaller (**1a**, **1g**, **1m**) or bulkier (**1u**, **1ae**) substituents in position 7. They displayed different (**1g**, **1ae**) or comparable (**1a**, **1m**, **1u**) inhibition activities against human and mycobacterial ADK. We tested their competition with adenosine and ATP γ S in the presence of either *hADK* or Mtb ADK. All selected 7-deazaadenosines selectively competed with adenosine, as their STD enhancements were significantly reduced, but did not affect ATP γ S signals in the presence of *hADK*. This suggests significantly lower affinity of tested compounds to ATP site relative to ATP γ S. The ATP site was occupied by **1a** in our crystal structure of *hADK*, but this was due to high inhibitor excess in the crystallization experiment. However, the STD data in the presence of Mtb ADK indicated strong competition of inhibitors with both substrates (Figure 3D,E), which confirmed that these compounds can also bind into the ATP site. The STD enhancements for the substrates and inhibitors normalized to the H-1' signal enhancement are shown in Table 2. We observed that H-1' is subjected to the strongest STD enhancement for all inhibitors tested, independent of the protein present in sample solution. This suggests that the sugar moiety is in direct contact with the protein in all complexes. The substantial contributions from the purine protons H-2 and H-8 are found in all complexes, with approximately 50% enhancement relative to H-1'. Protein-dependent differences were found in the STD enhancements of the signals from substituents at position 7. The relative enhancements for aromatic substituent signals were higher than H-2 and H-8 enhancements in *hADK* complexes, while they remained comparable in Mtb ADK complexes, suggesting that the substituents maintain much more extensive contacts with *hADK* than Mtb ADK. The potential binding of 7-deazanucleosides into the ATP binding site contributes to the loss of their phosphorylation.

Binding of Selected 7-Hetaryl-7-deazapurine Derivatives to Human ADK by Protein-Detected NMR. We used two-dimensional NMR spectroscopy to study the detailed mechanism of inhibitor binding to *hADK*. The low stability of Mtb ADK at the high concentration (100 μ M) required for relatively long NMR experiments did not allow us to prepare a sample of sufficient quality for binding experiments. Initially, we analyzed 2D $^{15}\text{N}/^1\text{H}$ HSQC spectra of reference samples of ^{15}N -labeled *hADK* in the absence and presence of adenosine or ATP γ S. The 2D $^{15}\text{N}/^1\text{H}$ HSQC spectrum of free *hADK* consisted of 270 unique signals from backbone and side chain amide groups, some subjected to extensive spectral overlaps, which corresponds to the size of the analyzed protein. Both

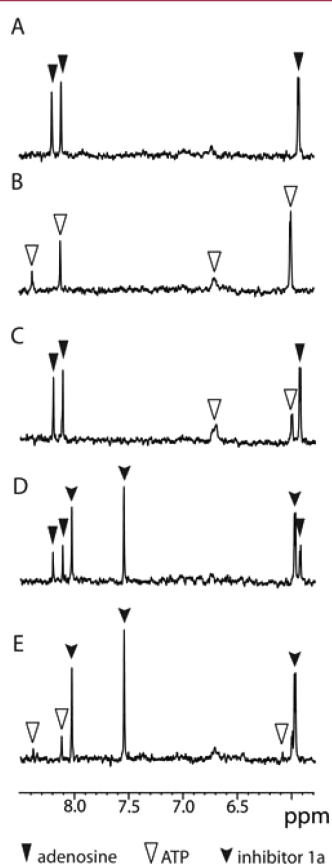


Figure 3. 1D ^1H STD NMR substrate/inhibitor competition experiments for Mtb ADK. (A) shows a region of the STD spectrum obtained for Mtb ADK in the presence of adenosine, while (B) shows the spectrum for the enzyme in the presence of ATP γ S. (C) shows the spectrum for the mixture of substrates, with intensity of the ATP γ S specific signals significantly reduced. (D) and (E) show competition of **1a** with adenosine and ATP γ S illustrated by the clear drops in the STD enhancement of signals from both substrates.

ligands induced a number of specific changes in the positions of signals in 2D $^{15}\text{N}/^1\text{H}$ HSQC spectra, indicating that this approach is suitable for studying binding modes of *h*ADK inhibitors.

Preliminary NMR experiments using ^{15}N labeled material revealed a relatively poor long-term stability of *h*ADK at temperatures above 25 °C. The 3D experiments required for backbone resonance assignment were acquired at 25 °C to minimize protein precipitation and overall material consumption. The exchange of nonlabile protons for deuterons enabled sequence-specific backbone resonance assignments; however, a certain proportion of amide groups unexpectedly did not back-exchange during protein purification in an H₂O environment and remained deuterated, as suggested by comparison of the 2D $^{15}\text{N}/^1\text{H}$ HSQC spectra obtained from ^{15}N and $^2\text{H}/^{13}\text{C}/^{15}\text{N}$ -labeled *h*ADK. The high quality of NMR spectra allowed us to assign essentially all 175 detectable signals in perdeuterated *h*ADK using a previously described approach.^{29,30} Detailed analysis revealed that the amide groups buried in the protein core and contributing as hydrogen bond donors were often not successfully protonated during purification in an H₂O environment. The distribution of successfully assigned backbone amide groups is illustrated in Figure S2.

As a next step, we acquired and analyzed 2D $^{15}\text{N}/^1\text{H}$ HSQC spectra of *h*ADK bound to the set of compounds (**1a,g,m,u,ae**) investigated by NMR 1D ^1H STD experiments. These data were compared with the reference spectra; we selected 17 well-resolved representative backbone amide signals in the spectrum of free *h*ADK (Table 3 and Figure 4). All compounds studied,

Table 3. Analysis of *h*ADK 2D $^{15}\text{N}/^1\text{H}$ HSQC Spectra in the Presence of Inhibitors^a

inhibitor	number of signals corresponding to the reference of			
	free <i>h</i> ADK	<i>h</i> ADK + adenosine	<i>h</i> ADK + ATP γ S	specific signal
1a	5	13	1	0
1g	3	14	1	0
1m	3	13	5	1
1u	5	11	3	2
1ae	6	6	8	2

^aWe selected a set of well-resolved backbone amide signals and followed their changes upon addition of selected inhibitors. Free *h*ADK and the *h*ADK in the presence of adenosine or ATP γ S were used as reference samples. The signals were sorted into four distinct categories according to their behavior in the presence of an inhibitor.

with the exception of **1ae**, which contains a large 4-phenoxythiinyl group, induced changes in 2D $^{15}\text{N}/^1\text{H}$ HSQC spectra that closely correspond to those observed for adenosine binding, suggesting direct competition of inhibitors for the adenosine binding pocket. The spectrum of *h*ADK in the presence of **1ae** exhibited signal changes that did not unambiguously correspond to any reference spectrum, indicating that the binding mode of this inhibitor might be atypical or mixed. Additional analysis using backbone resonance assignments revealed that this compound induced specific differences compared to the reference spectrum acquired for *h*ADK in the presence of adenosine. Similar data were obtained for the isopropylphenyl derivative (**1u**) with a relatively large substituent in position 7.

Quantum Mechanical Analysis of Binding of Selected 7-Hetaryl-7-deazapurine Derivatives to Human and Mtb ADK.

Complexes of *h*ADK and Mtb ADK with the compounds used for NMR competition experiments (**1a,g,m,u,ae**) were further analyzed using semiempirical quantum mechanical (SQM) based scoring function.^{31,32} To build in silico models of *h*ADK complexes, we used the X-ray structure of *h*ADK in complex with two adenosine molecules (PDB code 1BX4).²⁰ In this structure, one adenosine molecule is located in the adenosine binding site and the second in the ATP binding site. The inhibitors were built and scored in both binding sites. The complex of *h*ADK with **1ae** could not be built because of numerous steric clashes between the inhibitor and protein. The calculated scores for the remaining inhibitors are summarized in Table 4. The inhibitors have higher affinity to the adenosine binding site (scores from -30 to -65 kcal/mol) than to the ATP binding site (scores from -12 to -23 kcal/mol). This is due to the more favorable interactions in the adenosine binding site (ΔE_{int} more negative by about 60%). These results are in good agreement with our experimental NMR finding that the inhibitors compete with higher affinity with adenosine than with ATP in the presence of *h*ADK. Compounds **1a**, **1g**, and **1m** fit well into the adenosine binding site. The 7-deaza derivative **1u** is too big to fit into the conformation of *h*ADK that was used for modeling, and its binding requires changes in the protein conformation (see Figure S3). The conformational changes significantly increased the penalty for the change of the conformational “free” energies ($\Delta G^{\text{w}}_{\text{int}}$) of both the protein and ligand (by about 100% and 40%, respectively). This supports the NMR results showing that compounds with large substituents (**1u** and **1ae**) induce different structural changes in *h*ADK than adenosine or compounds with small substituents in position 7.

Mtb Adk complexes with the selected inhibitors were also studied using the SQM scoring function. Previous structural analyses of Mtb ADK show that binding of ATP or its analog does not change the conformation of this enzyme. However, the X-ray structure of Mtb ADK crystallized with **1a** (PDB code 4PVV) shows that the binding of adenosine analog results in movement of lid domain and formation of a semiclosed conformation. This suggests that inhibitors compete with adenosine in an open conformation. Subsequently, the binding affinity of the adenosine analogs to the adenosine site might increase when the conformation of Mtb ADK is changed from open to semiopen. To support this hypothesis, we used both the X-ray structure of Mtb ADK dimer in open conformation in complex with an ATP analog (PDB code 2PKN)²¹ and the X-ray structure of semiopen conformation of Mtb ADK crystallized with **1a** to build our in silico models of Mtb ADK complexes. The closed conformation of Mtb ADK (Mtb ADK dimer crystallized with adenosine, PDB code 2PKM) did not allow us to build models. The calculated scores are summarized in Table 5, and the SQM optimized complexes of **1a** and **1ae** are shown in Figure 5. Interestingly, the inhibitors have comparable affinity to both the adenosine and ATP binding sites in the open conformation of Mtb ADK (scores ranged from -20 to -25 and from -11 to -17 kcal/mol to the ATP and adenosine binding sites, respectively). However, the affinity of 7-substituted 7-deazapurine nucleosides to the adenosine binding site increases significantly in the semiopen conformation of Mtb ADK with bound nucleosides (score from -50 to -59 kcal/mol) and is comparable to those calculated for these inhibitors bound in *h*ADK adenosine site.

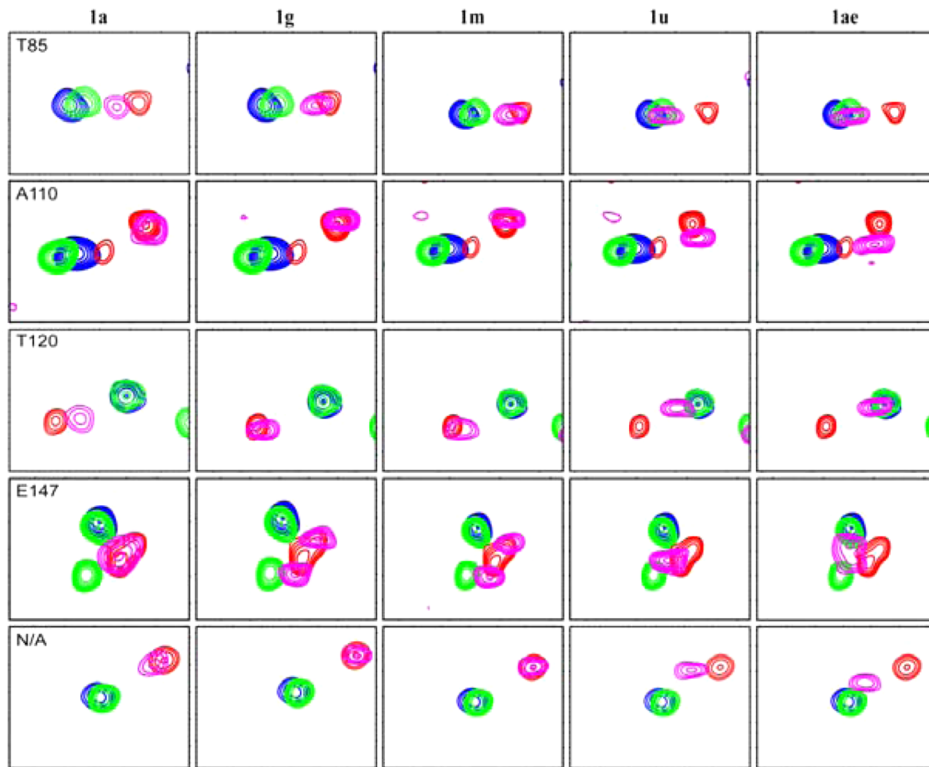


Figure 4. Binding of inhibitors to *h*ADK analyzed using 2D $^{15}\text{N}/^1\text{H}$ HSQC. Each row represents a different backbone amide group cross-peak (the residue number is given in the first column). Columns illustrate changes in the spectra obtained for a selected inhibitor. Contours are colored as follows: blue, free *h*ADK; green, *h*ADK in the presence of ATP γ S; red, *h*ADK in the presence of adenosine; magenta, *h*ADK in the presence of inhibitor. Concentration of all nucleosides was kept at 500 μM .

Table 4. Inhibition Constant (IC_{50}) and Score of the Studied Inhibitors to *h*ADK Calculated As a Sum of the Gas-Phase Interaction Energy (ΔE_{int}), the Interaction Solvation/Desolvation Free Energy ($\Delta\Delta G_{\text{solv}}$), the Change of the Conformational “Free” Energies of the Protein and Ligand ($\Delta G'^w_{\text{conf}}(\text{P},\text{L})$), and the Entropy Change upon Binding ($-T\Delta S_{\text{int}}$)

inhibitor	Human ADK						
	IC_{50} (μM)	score (kcal/mol)	ΔE_{int} (kcal/mol)	$\Delta\Delta G_{\text{solv}}$ (kcal/mol)	$\Delta G'^w_{\text{conf}}(\text{L})$ (kcal/mol)	$\Delta G'^w_{\text{conf}}(\text{P})$ (kcal/mol)	$-T\Delta S_{\text{int}}$ (kcal/mol)
Adenosine Binding Site							
1a	0.2 ± 0.015	-59.7	-149.6	59.3	7.6	23	0
1g	>5	-65.0	-158.4	61.3	8.6	23.5	0
1m	2.3 ± 0.17	-56.6	-157.2	61.3	9.1	30.1	0
1u	3.3 ± 0.4	-30.6	-163.9	68.1	11.5	49.7	4
ATP Binding Site							
1a	0.2 ± 0.015	-22.6	-93.5	43.8	2.4	24.7	0
1g	>5	-22.4	-97.1	47.3	2.5	24.8	0
1m	2.3 ± 0.17	-22.9	-95.8	49.4	2.2	21.3	0
1u	3.3 ± 0.4	-11.7	-101.5	52.7	4.6	28.5	4

CONCLUSIONS

A new series of 7-(het)aryl-7-deazaadenine ribonucleosides bearing small and bulky substituents in position 7 was synthesized and evaluated as potential new antimycobacterial agents. Several compounds bearing smaller substituents (e.g., **1a**) were found to inhibit both human and Mtb ADK and were cytotoxic, whereas several bulky derivatives (e.g., **1ad**, **1ae**, **1ag**) were specific inhibitors of the Mtb enzyme and were not cytotoxic. 7-(2-Naphthyl)-7-deazaadenine (**1f**) was the most active compound against Mtb strain My331/88 and drug-resistant strain Praha 131 *in vitro* (MIC = 2 or 4 μM , respectively), but its cytotoxicity disfavors its further development. The dibenzofuran derivative (**1ad**) had the best therapeutic index. This compound was a submicromolar Mtb-

ADK-specific inhibitor and was active against Mtb strains with a MIC of 4 $\mu\text{mol/L}$. This compound is a promising lead structure for further drug development. Following binding of the 7-(het)aryl-7-deazaadenine ribonucleosides into the adenosine site, Mtb ADK adopts a unique semiopen conformation of the lid domain, and *h*ADK adopts the closed conformation. Enzyme kinetics and 1D ^1H STD NMR analysis of the inhibitors’ competition with adenosine and ATP γ S showed that 7-(het)aryl-7-deazaadenine ribonucleosides bind preferentially into the adenosine site in *h*ADK and are readily accommodated in both, to the adenosine and ATP sites in Mtb ADK. Quantum mechanical analysis indicated that these compounds have higher affinity for the ATP site of Mtb ADK in the open conformation, but movement of the lid domain increases

Table 5. Inhibition Constant (IC_{50}) and Score of Inhibitors of Mtb ADK Calculated as a Sum of Gas-Phase Interaction Energy (ΔE_{int}), the Interaction Solvation/Desolvation Free Energy ($\Delta\Delta G_{solv}$), the Change in Conformational “Free” Energies of the Protein and Ligand ($\Delta G'^w_{conf}(P,L)$), and the Entropy Change upon Binding ($-T\Delta S_{int}$)

inhibitor	IC_{50} (μM)	score (kcal/mol)	ΔE_{int} (kcal/mol)	$\Delta\Delta G_{solv}$ (kcal/mol)	Mtb AdK		
					$\Delta G'^w_{conf}(L)$ (kcal/mol)	$\Delta G'^w_{conf}(P)$ (kcal/mol)	$-T\Delta S_{int}$ (kcal/mol)
Adenosine Binding Site in Semiopen Conformation							
1a	0.33 ± 0.02	-57.0	-131.3	63.3	2.9	8.1	0
1g	2.1 ± 0.15	-59.2	-140.7	66.9	3.4	11.3	0
1m	4.5 ± 0.2	-57.2	-141.5	68.0	4.9	11.4	0
1u	2.33 ± 0.25	-51.4	-140.8	69.5	3.8	12.1	4
1ae	0.3 ± 0.02	-49.8	-142.9	72.0	5.2	15.9	0
Adenosine Binding Site in Open Conformation							
1a	0.33 ± 0.02	-17.4	-72.5	44.4	4.4	6.3	0
1g	2.1 ± 0.15	-16.4	-77.8	47.3	5.3	8.9	0
1m	4.5 ± 0.2	-12.9	-72.3	48.8	2	8.6	0
1u	2.33 ± 0.25	-13.3	-77.5	44.7	5.4	10.1	4
1ae	0.3 ± 0.02	-11.4	-75.1	47.2	5.3	11.2	0
ATP Binding Site in Open Conformation							
1a	0.33 ± 0.02	-23.8	-76.2	43.6	0.9	8	0
1g	2.1 ± 0.15	-24.8	-78.8	45.5	1.1	7.4	0
1m	4.5 ± 0.2	-20.1	-75.4	44.6	1.3	9.4	0
1u	2.33 ± 0.25	-20.3	-84	46.1	2.9	10.7	4
1ae	0.3 ± 0.02	-24.3	-83.8	47.2	2.1	10.3	0

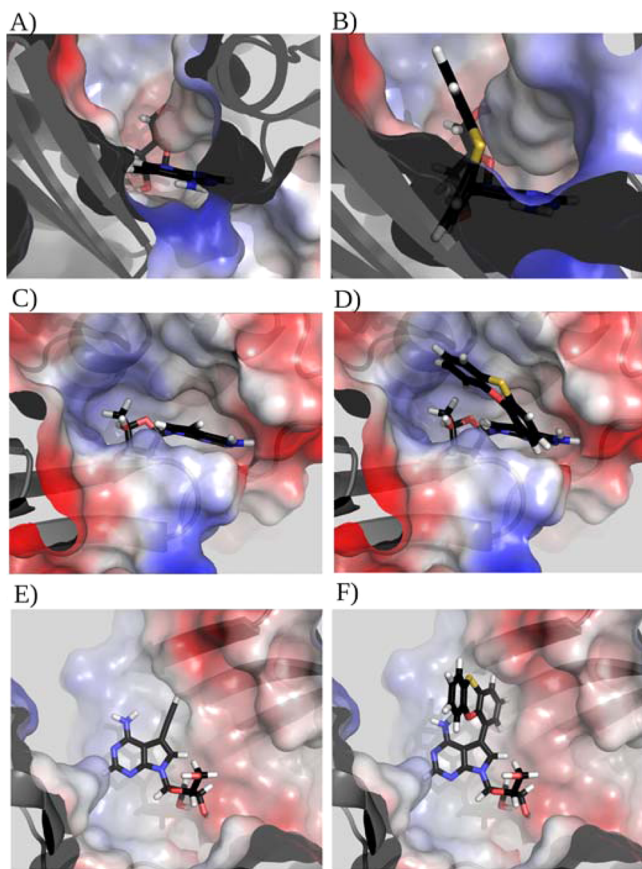


Figure 5. Model of **1a** bound to adenosine binding site in semiopen conformation (A), ATP binding site in open conformation (C) and adenosine binding site in open conformation (E) of Mtb ADK and **1ae** bound to adenosine binding site in semiopen conformation (B), ATP binding site in open conformation (D) and adenosine binding site in open conformation (F) of Mtb ADK.

binding affinity of these inhibitors in the adenosine site. Both the preferential binding of 7-(het)aryl-7-deazaadenine ribonucleosides in the Mtb ADK ATP binding site and the unique semiopen conformation of Mtb ADK during inhibitor binding in the adenosine site explain the observation that 7-(het)aryl-7-deazaadenine ribonucleosides are not phosphorylated by ADK. Similar mechanisms may also occur for deazaadenine ribonucleoside derivatives modified at other positions.

EXPERIMENTAL SECTION

Chemical Synthesis. **4-Amino-5-(3,4-dimethylphenyl)-7-(β -D-ribofuranosyl)-7H-pyrrolo[2,3-d]pyrimidine (1t).** An argon-purged mixture of 4-amino-5-iodo-7-(β -D-ribofuranosyl)-7H-pyrrolo[2,3-d]pyrimidine (**2**, 392 mg, 1 mmol), 3,4-dimethylphenylboronic acid (225 mg, 1.5 mmol), Na_2CO_3 (318 mg, 3 mmol), TPPTS (71 mg, 0.125 mmol), $Pd(OAc)_2$ (11 mg, 0.05 mmol) in water/MeCN (2:1, 5 mL) was stirred at 100 °C for 3 h. After cooling, the mixture was neutralized using aqueous HCl (1 M) and concentrated to dryness in vacuo. The residue was loaded onto silica by coevaporation from a chloroform/MeOH solution, and column chromatography (SiO_2 , 0 → 2.5% MeOH in $CHCl_3$) afforded **1t** (305 mg, 82%) as a yellowish foam. Mp 120–124 °C. $[\alpha]_D = -56.3$ (*c* 0.270, DMSO). 1H NMR (600.1 MHz, DMSO-*d*₆): 2.26 (s, 3H, CH₃-4); 2.28 (s, 3H, CH₃-3); 3.54 (bdt, 1H, $J_{gem} = 11.8$, $J_{5'b,4'} = J_{5'b,OH} = 3.5$, H-5'b); 3.63 (bdd, 1H, $J_{gem} = 11.8$, $J_{5'a,4'} = 3.5$, H-5'a); 3.91 (td, 1H, $J_{4',S'} = 3.5$, $J_{4',3'} = 3.2$, H-4'); 4.10 (ddd, 1H, $J_{3',2'} = 5.1$, $J_{3',OH} = 4.8$, $J_{3',4'} = 3.2$, H-3'); 4.45 (ddd, 1H, $J_{2',OH} = 6.5$, $J_{2',1'} = 6.3$, $J_{2',3'} = 5.1$, H-2'); 5.14 (d, 1H, $J_{OH,3'} = 4.8$, OH-3'); 5.22 (bm, 1H, OH-5'); 5.34 (d, 1H, $J_{OH,2'} = 6.6$, OH-2'); 6.11 (d, 1H, $J_{1',2'} = 6.3$, H-1'); 6.13 (bs, 2H, NH₂); 7.18 (dd, 1H, $J_{6,S} = 7.7$, $J_{6,2} = 2.0$, H-6-C₆H₃Me₂); 7.25 (d, 1H, $J_{5,6} = 7.7$, H-5-C₆H₃Me₂); 7.26 (d, 1H, $J_{2,6} = 2.0$, H-2-C₆H₃Me₂); 7.48 (s, 1H, H-6); 8.14 (s, 1H, H-2). ^{13}C NMR (150.9 MHz, DMSO-*d*₆): 19.33 (CH₃-4); 19.76 (CH₃-3); 61.92 (CH₂-5'); 70.88 (CH-3'); 74.01 (CH-2'); 85.32 (CH-4'); 87.21 (CH-1'); 100.82 (C-4a); 116.58 (C-5); 120.93 (CH-6); 126.06 (CH-6-C₆H₃Me₂); 129.88 (CH-2-C₆H₃Me₂); 130.27 (CH-5-C₆H₃Me₂); 132.11 (C-1-C₆H₃Me₂); 135.22 (C-4-C₆H₃Me₂); 137.10 (C-3-C₆H₃Me₂); 150.91 (C-7a); 151.81 (CH-2); 157.50 (C-4). IR (ATR): ν 1625, 1589, 1542, 1469, 1303, 1236, 1217, 1185, 1122, 1082, 1041, 896, 869, 828, 798, 707, 646 cm^{-1} . MS (ESI) *m/z* 371 (M + H), 393 (M + Na). HRMS (ESI) for $C_{19}H_{23}N_4O_4$ [M + H]⁺ calcd, 371.1714; found, 371.1713. Anal. (C₁₉H₂₂N₄O₄·0.8H₂O) C, H, N.

Other compounds (**1u–aj**) were prepared analogously. For characterization data, see Supporting Information.

Enzyme Preparation and Inhibitor Testing. Expression and purification of human and Mtb ADK were performed as previously described.¹⁹ Compounds were tested for inhibition of human and Mtb ADK using previously established methods.¹⁹

Enzyme Kinetics. The individual assays were performed at 37 °C in 96-well microtiter plates. The reactions with both enzymes were performed in 250 mM Tris, pH 8.0, 50 mM KCl, 5 mM MgCl₂. When inhibitor **1a** was tested for a possible competition with adenosine, the concentration of ATP in the reaction mixtures was fixed at 5 mM for Mtb ADK or 120 μM for hADK. The concentration of radiolabeled [³H]adenosine varied from 0 to 1 μM. During testing of inhibitor **1a** with ATP the concentration of radiolabeled adenosine was kept at 5 μM and concentration of ATP increased from 0 to 60 nM (hADK) or 0 to 0.5 mM (Mtb ADK). The individual reactions were started by the addition of enzyme, and the reaction proceeded for 4 min. Then 80 μL of samples was withdrawn and directly added to 1 mL of ice cold 0.1 M LaCl₃ to precipitate formed radiolabeled AMP. After keeping on ice for at least 3 h, the precipitate was collected by filtration on a glass-microfiber filter (1.2 μm pores, Sigma-Aldrich). The filters were washed with 100 mL of ice cold water, dried, and the radioactivity was measured in a liquid scintillation counter (Tri-Carb 2900 TR) after adding of 4 mL of scintillation cocktail. Two or three separate measurements were performed for best fitting the experimental data. The obtained results were analyzed using SigmaPlot (version 11) and Microsoft Excel software.

Antimycobacterial Susceptibility Testing. Compounds were tested for antimycobacterial activity against Mtb 331/88 (H37Rv) and patient-derived MDR Mtb strain Praha 131 as previously described.³³ Micromethod was used to determine the minimum inhibitory concentration (MIC). MIC values were determined after incubation at 37 °C for 14 and 21 days. The first-line anti-TB drug isoniazid (INH) was used as a reference compound.

NMR Spectroscopy. All NMR data were collected on a 600 MHz Bruker Avance spectrometer equipped with a triple-resonance (¹⁵N/¹³C/¹H) cryoprobe. NMR samples were prepared in a 25 mM sodium (hADK) or potassium (Mtb ADK) phosphate, 15 mM MgCl₂, 100 mM sodium chloride buffer at pH 7.0, containing 5% D₂O/95% H₂O. NMR spectra for resonance assignment of hADK were acquired from 0.35 mL samples of 0.25 mM ²H/¹³C/¹⁵N protein at 25 °C. A series of triple-resonance spectra were recorded to determine sequence-specific resonance assignments for hADK. In particular, we used TROSY versions of HNCACB, HN(CO)CACB, HNCA, HNCO, and HN(CA)CO experiments^{34,35} with typical acquisition times of 7 ms for ¹³C^{a/b}, 30 ms for ¹³C', 16 ms for ¹⁵N, and 70 ms for ¹H. The total experimental times for 3D experiments were 48–96 h.

Uniformly ¹⁵N and ²H/¹³C/¹⁵N labeled hAdk was produced from cells grown in minimal medium containing ¹⁵N-ammonium sulfate and ¹³C-D-glucose if required, as the sole nitrogen and carbon sources, and 100% D₂O when appropriate as described previously.³⁶ The specific binding of small molecule substrates or inhibitors to hADK was monitored by changes induced in the positions of signals of 75 μM ¹⁵N-labeled hADK in 2D ¹⁵N/¹H HSQC spectra acquired at 35 °C. In addition, the binding of small molecules to either hADK or Mtb ADK was followed by ligand-detected saturation transfer difference (STD) experiments.^{37,38} STD spectra were acquired at 20 °C using 0.55 mL samples of 5 μM unlabeled hADK or Mtb ADK in the presence of a 100-fold excess (500 μM) of small molecule substrates or inhibitors with 2.5 s irradiation alternating between 0.5 ppm (on-resonance) and 20 ppm (off-resonance) using a train of 50 ms Gaussian pulses. The typical experimental time was 14 min.

Quantum Mechanical Analysis. To build *in silico* models, we used the X-ray structure of hADK in complex with two adenosine molecules (PDB code 1BX4),²⁰ Mtb ADK crystallized with **1a** (PDB code 4PVV), and the X-ray structure of Mtb ADK dimer in open conformation in complex with an ATP analog (PDB code 2PKN).²¹ The complexes were systematically optimized using the PM6-D3H4 method³⁹ combined with the COSMO solvent model⁴⁰ and fire algorithm. We only optimized amino acids within 8 Å of the inhibitors.

The rest of the protein was frozen. The binding affinity was approximated by the total score expressed by eq 1.^{31,32}

$$\text{score} = \Delta E_{\text{int}} + \Delta \Delta G_{\text{solv}} + \Delta G'^{\text{w}}_{\text{conf}}(\text{L}) + \Delta G'^{\text{w}}_{\text{conf}}(\text{P}) - T \Delta S_{\text{int}} \quad (1)$$

$$\Delta \Delta G_{\text{solv}} = \Delta \Delta G_{\text{int,solv}} + (\Delta G^{\text{low}}_{\text{solv}}(\text{L}) - \Delta G^{\text{high}}_{\text{solv}}(\text{L})) \quad (2)$$

Particular terms in the equation describe the gas-phase interaction energy (ΔE_{int}), the interaction solvation/desolvation free energy ($\Delta \Delta G_{\text{solv}}$), the change of the conformational “free” energy of ligand and protein ($\Delta G'^{\text{w}}_{\text{conf}}(\text{L}, \text{P})$), and the entropy change upon binding ($T \Delta S_{\text{int}}$). The ΔE_{int} was calculated using the PM6-D3H4 method. The solvation free-energy change $\Delta \Delta G_{\text{int,solv}}$ was determined by the COSMO solvent model. The more accurate SMD/HF/6-31G* method was also used.^{41,42} However, the SMD method is too demanding to be used for a protein, giving rise to the correction of ligand solvation/desolvation ($\Delta G^{\text{low}}_{\text{solv}}(\text{L}) - \Delta G^{\text{high}}_{\text{solv}}(\text{L})$), which is the difference between the solvation free energy calculated at high (SMD/HF/6-31G*) and low (COSMO/PM6) levels of theory.

The $\Delta G'^{\text{w}}_{\text{conf}}(\text{L}, \text{P})$ term is the “free” energy change between the ligand and protein in their optimal solution structure and the conformation they adopt in the complex. To evaluate $\Delta G'^{\text{w}}_{\text{conf}}(\text{L})$, we combined the gas phase PM6-D3H4 energy with the SMD solvation free energy. The $G'^{\text{w}}_{\text{conf}}(\text{P})$ term was evaluated using an annealing approach at the molecular mechanics level. The parameters for the protein were obtained from the FF03 force field; parameters for the inhibitors were obtained from the GAFF force field. The charges for the ligands were calculated using the RESP procedure at the HF/6-31G* level as recommended.⁴³ The isolated protein and the complex were optimized by annealing prior to standard optimization using fire algorithm. The annealing was started at 300 K, then cooled to 0 K in 1000 steps (length of each step, 1 fs) using Berendsen thermostat. For each system, eight independent runs with different starting velocities were performed, and the obtained energies were averaged. Only residues within 8 Å of the inhibitors were optimized. The rest of the protein was frozen. Finally, the $T \Delta S_{\text{int}}$ term of score was estimated using the rotatable bonds approach (i.e., 1 kcal/mol penalty for each rotatable bond in the ligand).

Protein Crystallization. For crystallization experiments at 19 °C, hADK at a concentration of 10 mg/mL and Mtb ADK at a concentration of 20 mg/mL in buffer containing 20 mM Tris-Cl, pH 7.4, and 5 mM 2-mercaptoethanol were used. Prior to setting up crystallization experiments, proteins were preincubated with 5 mM **1a** for 1 h at room temperature. Initial crystallization trials were performed with the help of a Gryphon crystallization workstation (Art Robbins) by the sitting drop vapor diffusion method in 96-well plates; 0.2 μL of protein solution was mixed with 0.2 μL of reservoir solution, and the drop was equilibrated against 200 μL of reservoir solution. The PEGs Suite and JSCG Core I Suite (QIAGEN) were used for the initial crystallization condition screen. Initial microcrystals appeared in several days. Further optimization involved changing to the hanging drop mode in 24-well crystallization plates (EasyXtal DG-Tool, QIAGEN). Optimal crystals of the hADK-**1a** complex were obtained by mixing 2 μL of protein solution with 2 μL of reservoir solution composed of 0.2 M MgCl₂ and 20% (w/v) PEG 3350. Crystals of the Mtb ADK-**1a** complex were obtained by mixing 3 μL of protein solution with 1 μL of reservoir solution composed of 0.1 M sodium acetate, pH 4.6, and 15% (w/v) PEG 20 000.

Data Collection and Structure Determination. For data collection, the crystals were soaked in reservoir solution supplemented with 20% (v/v) glycerol and transferred into liquid nitrogen. Diffraction data were collected at 100 K at BESSY beamline 14.2⁴⁴ in Berlin, Germany, using an MAR Mosaic 225 CCD detector. The crystals of hADK and Mtb ADK in complex with **1a** diffracted up to 2.5 Å resolution. Diffraction data for hADK in complex with **1a** were integrated and reduced using MOSFLM⁴⁵ and scaled using SCALA.⁴⁶ The MtbADK-**1a** crystals were of problematic character whose quality could not be optimized despite a great effort, and diffraction pattern contained extra reflections. The scaling of experimental frames and

empirical absorption correction was done with CrysAlisPro (Agilent Technologies, version 1.171.37.34) using the symmetry *P3*. Finally, the symmetry equivalent reflections were merged by JANA2006⁴⁷ and resulting reflection file was converted to the mtz format using CCP4 program suite.⁴⁸ Details of the data processing procedure are given in the Supporting Information. Crystal parameters and data collection statistics are summarized in Table S1.

The structure of the hADK-1a complex was solved by molecular replacement using the coordinates from PDB entry 1BX4²⁰ as the initial model. The structure of the Mtb ADK-1a complex was solved by molecular replacement using coordinates from PDB entry 2PKM⁵ as the initial model. Automated rebuilding was performed with the program Buccaneer.⁴⁹ Restrained refinement to 2.5 Å resolution was performed using the program REFMAC.⁵⁰ The merohedric twinning was taken into the account during rebuilding and refinement. Coot program was used for inhibitor fitting, manual rebuilding of protein chain, and addition of water molecules. Atomic coordinates and a geometry library for the inhibitor were generated using the PRODRG server.⁵¹

ASSOCIATED CONTENT

Supporting Information

Synthetic procedures and characterization data for all new compounds, additional figures, and crystallographic data. This material is available free of charge via the Internet at <http://pubs.acs.org>.

Accession Codes

Atomic coordinates and structure factors for the crystal structures of hADK-1a and Mtb ADK-1a have been deposited in the PDB with accession codes 4O1L and 4PVV, respectively.

AUTHOR INFORMATION

Corresponding Authors

*M.H.: e-mail, hocek@uochb.cas.cz; phone, +420 220183324.

*I.P.: e-mail, pichova@uochb.cas.cz; phone, +420 220183251.

Author Contributions

#J.S. and P.N. contributed equally.

Notes

The authors declare no competing financial interest.

∞I.V.: Deceased on May 25, 2014.

ACKNOWLEDGMENTS

This work was supported by EU-PF7 SysteMtb Collaborative Project 241587, Grant P207/11/0344 from the Czech Science Foundation, RVO 61388963 Project, Project InterBioMed LO1302, Programme "NAVRAT" LK11205 and CEITEC—open access project, No. LM2011020 from the Ministry of Education of the Czech Republic, and IOCB-Gilead Research Centre. We thank Dagmar Grundová for excellent technical assistance and H. Hoffman for editing of the manuscript.

ABBREVIATIONS USED

ADK, adenosine kinase; ATPγS, adenosine 5'-[γ -thio]-triphosphate; MDR, multidrug-resistant; XDR, extensively drug-resistant; CC₅₀, 50% cytotoxic concentration; IC₅₀, 50% inhibitory concentration; STD, saturation transfer difference; HSQC, heteronuclear single quantum coherence

REFERENCES

- (1) Gandhi, N. R.; Nunn, P.; Dheda, K.; Schaaf, H. S.; Zignol, M.; van Soolingen, D.; Jensen, P.; Bayona, J. Multidrug-resistant and extensively drug-resistant tuberculosis: a threat to global control of tuberculosis. *Lancet* **2010**, *375*, 1830–1843.

(2) Niemi, M.; Backman, J. T.; Fromm, M. F.; Neuvonen, P. J.; Kivistö, K. T. Pharmacokinetic interactions with rifampicin: clinical relevance. *Clin. Pharmacokinet.* **2003**, *42* (9), 819–850.

(3) Parker, W. B.; Long, M. C. Purine metabolism in *Mycobacterium tuberculosis* as a target for drug development. *Curr. Pharm. Des.* **2007**, *13*, 599–608.

(4) Ducati, R. G.; Breda, A.; Basso, A.; Basso, L. A.; Santos, D. S. Purine salvage pathway in *Mycobacterium tuberculosis*. *Curr. Med. Chem.* **2011**, *18*, 1258–1275.

(5) Reddy, M. C. M.; Palaninathan, S. K.; Shetty, N. D.; Owen, J. L.; Watson, M. D.; Sacchettini, J. C. High resolution crystal structures of *Mycobacterium tuberculosis* adenosine kinase: insights into the mechanism and specificity of this novel prokaryotic enzyme. *J. Biol. Chem.* **2007**, *282*, 27334–27342.

(6) Long, M. C.; Escuyer, V.; Parker, W. B. Identification and characterization of a unique adenosine kinase from *Mycobacterium tuberculosis*. *J. Bacteriol.* **2003**, *185* (22), 6548–6555.

(7) Muchmore, S. W.; Smith, R. A.; Stewart, A. O.; Cowart, M. D.; Gomtsyan, A.; Mamulenko, M. A.; Yu, H.; Severin, J. M.; Bhagwat, S. S.; Lee, C. H.; Kowaluk, E. A.; Narcis, M. F.; Jakob, C. L. Crystal structures of human adenosine kinase inhibitor complexes reveal two distinct binding modes. *J. Med. Chem.* **2006**, *49* (23), 6726–6731.

(8) Al Safarjalani, O. N.; Rais, R. H.; Kim, Y. A.; Chu, C. K.; Naguib, F. N.; El Kouni, M. H. Carbocyclic 6-benzylthioinosine analogues as subversive substrates of *Toxoplasma gondii* adenosine kinase: biological activities and selective toxicities. *Biochem. Pharmacol.* **2010**, *80*, 955–963.

(9) Boison, D. Adenosine kinase: exploitation for therapeutic gain. *Pharmacol. Rev.* **2013**, *65*, 1–39.

(10) Barrow, E. W.; Westbrook, L.; Bansal, N.; Suling, W. J.; Maddry, J. A.; Parker, W. B.; Barrow, W. W. Antimycobacterial activity of 2-methyl-adenosine. *J. Antimicrob. Chemother.* **2003**, *52* (5), 801–808.

(11) Ugarkar, B. G.; DaRe, J. M.; Kopcho, J. J.; Browne, C. E., III; Schanzer, J. M.; Wiesner, J. B.; Erion, M. D. Adenosine kinase inhibitors. 1. Synthesis, enzyme inhibition and antiseizure activity of 5-iodotubercidin analogues. *J. Med. Chem.* **2000**, *43*, 2883–2893.

(12) Ugarkar, B. G.; Castellino, A. J.; DaRe, J. S.; Ramirez-Weinhouse, M.; Kopcho, J. J.; Rosengren, S.; Erion, M. D. Adenosine kinase inhibitors. 3. Synthesis, SAR and antiinflammatory activity of a series of L-lyxofuranosyl nucleosides. *J. Med. Chem.* **2003**, *46*, 4750–4760.

(13) Kim, Y. A.; Sharon, A.; Chu, C. K.; Rais, R. H.; Al Safarjalani, O. N.; Naguib, F. N. M.; el Kouni, M. H. Structure–activity relationships of 7-deaza-6-benzylthioinosine analogues as ligands of *Toxoplasma gondii* adenosine kinase. *J. Med. Chem.* **2008**, *51*, 3934–3945.

(14) Ugarkar, B. G.; Castellino, A. J.; DaRe, J. M.; Kopcho, J. J.; Wiesner, J. B.; Schanzer, J. M.; Erion, M. D. Adenosine kinase inhibitors. 2. Synthesis, enzyme inhibition and antiseizure activity of diaryltubercidin analogues. *J. Med. Chem.* **2000**, *43*, 2894–2905.

(15) Boyer, S. H.; Ugarkar, B. G.; Solbach, J.; Kopcho, J.; Matelich, M. C.; Ollis, K.; Gomez-Galeno, J. E.; Mendonca, R.; Tsuchiya, M.; Nagahisa, A.; Nakane, M.; Wiesner, J. B.; Erion, M. D. Adenosine kinase inhibitors. 5. Synthesis, enzyme inhibition and analgesic activity of erythrodiaryltubercidin analogs. *J. Med. Chem.* **2005**, *48*, 6430–6441.

(16) Nauš, P.; Pohl, R.; Votruba, I.; Džubák, P.; Hajdúch, M.; Ameral, R.; Birkus, G.; Wang, T.; Ray, A. S.; Mackman, R.; Cihlář, T.; Hocek, M. 6-(Heteroaryl)-7-deazapurine ribonucleosides as novel potent cytostatic agents. *J. Med. Chem.* **2010**, *53*, 460–470.

(17) Perlíková, P.; Konečný, P.; Nauš, P.; Snášel, J.; Votruba, I.; Džubák, P.; Pichová, I.; Hajdúch, M.; Hocek, M. 6-Alkyl-, 6-aryl- or 6-hetaryl-7-deazapurine ribonucleosides as inhibitors of human or MTB adenosine kinase and potential antimycobacterial agents. *Med. Chem. Commun.* **2013**, *4*, 1497–1500.

(18) Bourderiou, A.; Nauš, P.; Perlíková, P.; Pohl, R.; Pichová, I.; Votruba, I.; Džubák, P.; Konečný, P.; Hajdúch, M.; Stray, K. M.; Wang, T.; Ray, A. S.; Feng, J. Y.; Birkus, G.; Cihlář, T.; Hocek, M. Synthesis and significant cytostatic activity of 7-hetaryl-7-deazaadenosines. *J. Med. Chem.* **2011**, *54*, 5498–5507.

- (19) Spáčilová, P.; Nauš, P.; Pohl, R.; Votruba, I.; Snášel, J.; Zábranská, H.; Pichová, I.; Ameral, R.; Birkuš, G.; Cihlář, T.; Hocek, M. CycloSal-phosphate pronucleotides of cytostatic 6-(het)aryl-7-deazapurine ribonucleosides: synthesis, cytostatic activity, and inhibition of adenosine kinases. *ChemMedChem* **2010**, *5*, 1386–1396.
- (20) Mathews, I. L.; Erion, M. D.; Ealick, S. E. Structure of human adenosine kinase at 1.5 Å resolution. *Biochemistry* **1998**, *37*, 15607–20.
- (21) Reddy, M. C. M.; Palaninathan, S. K.; Shetty, N. D.; Owen, J. L.; Watson, M. D.; Sacchettini, J. C. High resolution crystal structures of *Mycobacterium tuberculosis* adenosine kinase. *J. Biol. Chem.* **2007**, *282*, 27334–27342.
- (22) Gribble, F. M.; Loussouarn, G.; Tucker, S. J.; Zhao, C.; Nichols, C. G.; Ashcroft, F. M. A novel method for measurement of submembrane ATP concentration. *J. Biol. Chem.* **2000**, *275*, 30046–30049.
- (23) Larcombe-McDouall, J.; Buttell, N.; Harrison, N.; Wray, S. In vivo pH and metabolite changes during a single contraction in rat uterine smooth muscle. *J. Physiol.* **1999**, *518*, 783–790.
- (24) Dragon, S.; Hille, R.; Gotz, R.; Baumann, R. Adenosine 3':5'-cyclic monophosphate (cAMP) inducible pyrimidine 5'-nucleotidase and pyrimidine nucleotide metabolism of chicken embryonic erythrocytes. *Blood* **1998**, *91*, 3052–3058.
- (25) Kawashima, S. Inhibition of rat liver transglutaminase by nucleotides. *Experientia* **1991**, *47*, 709–712.
- (26) Koul, A.; Vranckx, L.; Dendouga, N.; Balemans, W.; van den Wyngaert, I.; Vergauwen, K.; Göhlmann, H. W.; Willebrods, R.; Poncellet, A.; Guillemont, J.; Bald, D.; Andries, K. Diarylquinolines are bactericidal for dormant mycobacteria as a result of disturbed ATP homeostasis. *J. Biol. Chem.* **2008**, *283* (37), 25273–25280.
- (27) Park, J.; Gupta, R. S. Adenosine kinase and ribokinase—the RK family of proteins. *Cell. Mol. Life Sci.* **2008**, *65* (18), 2875–2896.
- (28) Rao, S. P. S.; Alonso, S.; Rand, L.; Pethe, K. The protonmotive force is required for maintaining ATP homeostasis and viability of hypoxic, nonreplicating *Mycobacterium tuberculosis*. *Proc. Natl. Acad. Sci. U.S.A.* **2008**, *105*, 11945–11950.
- (29) Renshaw, P. S.; Veverka, V.; Kelly, G.; Frenkel, T. A.; Williamson, R. A.; Gordon, S. V.; Hewinson, R. G.; Carr, M. D. Sequence-specific assignment and secondary structure determination of the 195-residue complex formed by the *Mycobacterium tuberculosis* proteins CFP-10 and ESAT-6. *J. Biomol. NMR* **2004**, *30*, 225–226.
- (30) Veverka, V.; Lennie, G.; Crabbe, T.; Bird, I.; Taylor, R. J.; Carr, M. D. NMR assignment of the mTOR domain responsible for rapamycin binding. *J. Biomol. NMR* **2006**, *36*, 3–3.
- (31) Fanfrlik, J.; Bronowska, A. K.; Režáč, J.; Přenosil, O.; Konvalinka, J.; Hobza, P. A reliable docking/scoring scheme based on the semiempirical quantum mechanical PM6-DH2 method accurately covering dispersion and H-bonding: HIV-1 protease with 22 ligands. *J. Phys. Chem. B* **2010**, *114*, 12666–12678.
- (32) Lepšík, M.; Řežáč, J.; Kolař, M.; Pecina, A.; Hobza, P.; Fanfrlik, J. The semiempirical quantum mechanical scoring function for in-silico drug design. *ChemPlusChem* **2013**, *78*, 921–931.
- (33) Krátký, M.; Vinšová, J.; Novotná, E.; Mandíková, J.; Wsól, V.; Trejtnar, F.; Ulmann, V.; Stolaříková, J.; Fernandes, S.; Bhat, S.; Liu, J. O. Salicylanilide derivatives block *Mycobacterium tuberculosis* through inhibition of isocitrate lyase and methionine aminopeptidase. *Tuberculosis* **2012**, *92* (5), 434–439.
- (34) Salzmann, M.; Wider, G.; Pervushin, K.; Senn, H.; Wuthrich, K. TROSY-type triple-resonance experiments for sequential NMR assignments of large proteins. *J. Am. Chem. Soc.* **1999**, *121*, 844–848.
- (35) Eletsky, A.; Kienhofer, A.; Pervushin, K. TROSY NMR with partially deuterated proteins. *J. Biomol. NMR* **2001**, *20*, 177–180.
- (36) Wilkinson, I. C.; Hall, C. J.; Veverka, V.; Shi, J. Y.; Muskett, F. W.; Stephens, P. E.; Taylor, R. J.; Henry, A. J.; Carr, M. D. High resolution NMR-based model for the structure of a scFv-IL-1 beta complex potential for NMR as a key tool in therapeutic antibody design and development. *J. Biol. Chem.* **2009**, *284*, 31928–31935.
- (37) Salzmann, M.; Pervushin, K.; Wider, G.; Senn, H.; Wuthrich, K. TROSY in triple-resonance experiments: new perspectives for sequential NMR assignment of large proteins. *Proc. Natl. Acad. Sci. U.S.A.* **1998**, *95*, 13585–13590.
- (38) Mayer, M.; Meyer, B. Group epitope mapping by saturation transfer difference NMR to identify segments of a ligand in direct contact with a protein receptor. *J. Am. Chem. Soc.* **2001**, *123*, 6108–6117.
- (39) Řežáč, J.; Hobza, P. Advanced corrections of hydrogen bonding and dispersion for semiempirical quantum mechanical methods. *J. Chem. Theory Comput.* **2012**, *8*, 141–151.
- (40) Klamt, A.; Schuurmann, G. COSMO: a new approach to dielectric screening in solvents with explicit expressions for the screening energy and its gradient. *J. Chem. Soc., Perkin Trans. 2* **1993**, *5*, 799–805.
- (41) Marenich, A. V.; Cramer, C. J.; Truhlar, D. G. Universal solvation model based on solute electron density and on a continuum model of the solvent defined by the bulk dielectric constant and atomic surface tensions. *J. Phys. Chem. B* **2009**, *113*, 6378–6396.
- (42) Frisch, M. J.; Trucks, G. W.; Schlegel, H. B.; Scuseria, G. E.; Robb, M. A.; Cheeseman, J. R.; Scalmani, G.; Barone, V.; Mennucci, B.; Petersson, G. A.; Nakatsuji, H.; Caricato, M.; Li, X.; Hratchian, H. P.; Izmaylov, A. F.; Bloino, J.; Zheng, G.; Sonnenberg, J. L.; Hada, M.; Ehara, M.; Toyota, K.; Fukuda, R.; Hasegawa, J.; Ishida, M.; Nakajima, T.; Honda, Y.; Kitao, O.; Nakai, H.; Vreven, T.; Montgomery, J. A., Jr.; Peralta, J. E.; Ogliaro, F.; Bearpark, M.; Heyd, J. J.; Brothers, E.; Kudin, K. N.; Staroverov, V. N.; Kobayashi, R.; Normand, J.; Ragahavachari, K.; Rendell, A.; Burant, J. C.; Iyengar, S. S.; Tomasi, J.; Cossi, M.; Rega, N.; Millam, N. J.; Klene, M.; Knox, J. E.; Cross, J. B.; Bakken, V.; Adamo, C.; Jaraillo, J.; Gomperts, R.; Stratmann, R. E.; Yazayev, O.; Austin, A. J.; Cammi, R.; Pomelli, C.; Ochterski, J. W.; Martin, R. L.; Morokuma, K.; Zakrzewski, V. G.; Voth, G. A.; Salvador, P.; Dannenberg, J. J.; Dapprich, S.; Daniels, A. D.; Farkas, Ö.; Foresman, J. B.; Ortiz, J. V.; Cioslowski, J.; Fox, D. J. *Gaussian 09*; Gaussian, Inc.: Wallingford CT, 2009.
- (43) Case, D. A.; Darden, T. A.; Cheatham, T. E., III; Simmerling, C. L.; Wang, J.; Duke, R. E.; Luo, R.; Crowley, M.; Walker, R. C.; Zhang, W.; Merz, K. M.; Wang, B.; Hayik, S.; Roitberg, A.; Seabra, G.; Kolossvary, I.; Wong, K. F.; Paesani, F.; Vanicek, J.; Wu, X.; Brozell, S. R.; Steinbrecher, T.; Gohlke, H.; Yang, L.; Tan, C.; Mongan, J.; Hornak, V.; Cui, G.; Mathews, D. H.; Seetin, M. G.; Sagui, C.; Babin, V.; and Kollman, P. A. *AMBER 10*; University of California: San Francisco, CA, 2008.
- (44) Mueller, U.; Darowski, N.; Fuchs, M. R.; Foerster, R.; Hellwig, M.; Paithankar, S.; Puehringer, S.; Steffien, M.; Zocher, G.; Weiss, M. S. Facilities for macromolecular crystallography at the Helmholtz-Zentrum Berlin. *J. Synchrotron Radiat.* **2012**, *19*, 442–449.
- (45) Leslie, A. G. W. The integration of macromolecular diffraction data. *Acta Crystallogr.* **2006**, *D62*, 48–57.
- (46) Evans, P. Scaling and assessment of data quality. *Acta Crystallogr.* **2006**, *D62*, 72–82.
- (47) Petricek, V.; Dusek, M.; Palatinus, L. Crystallographic computing system JANA2006: general features. *Z. Kristallogr.* **2006**, *229*, 345–352.
- (48) Winn, M. D.; Ballard, C. C.; Cowtan, K. D.; Dodson, E. J.; Emsley, P.; Evans, P. R.; Keegan, R. M.; Krissinel, E. B.; Leslie, A. G. W.; McCoy, A.; McNicholas, S. J.; Murshudov, G. N.; Pannu, N. S.; Potterton, E. A.; Powell, H. R.; Read, R. J.; Vagin, A.; Wilson, K. S. Overview of the CCP4 suite and current developments. *Acta Crystallogr.* **2011**, *D67*, 235–242.
- (49) Cowtan, K. The Buccaneer software for automated model building. 1. Tracing protein chains. *Acta Crystallogr., Sect. D: Biol. Crystallogr.* **2006**, *62*, 1002–1011.
- (50) Emsley, P.; Cowtan, K. Coot: model building tools for molecular graphics. *Acta Crystallogr., Sect. D: Biol. Crystallogr.* **2004**, *60*, 2126–2132.
- (51) Schuettelkopf, A. W.; van Aalten, D. M. F. PRODRG—a tool for high-throughput crystallography of protein–ligand complexes. *Acta Crystallogr.* **2006**, *D60*, 1355–1363.